Met Office

Predictability barriers and diabatic processes during NAWDEX campaign

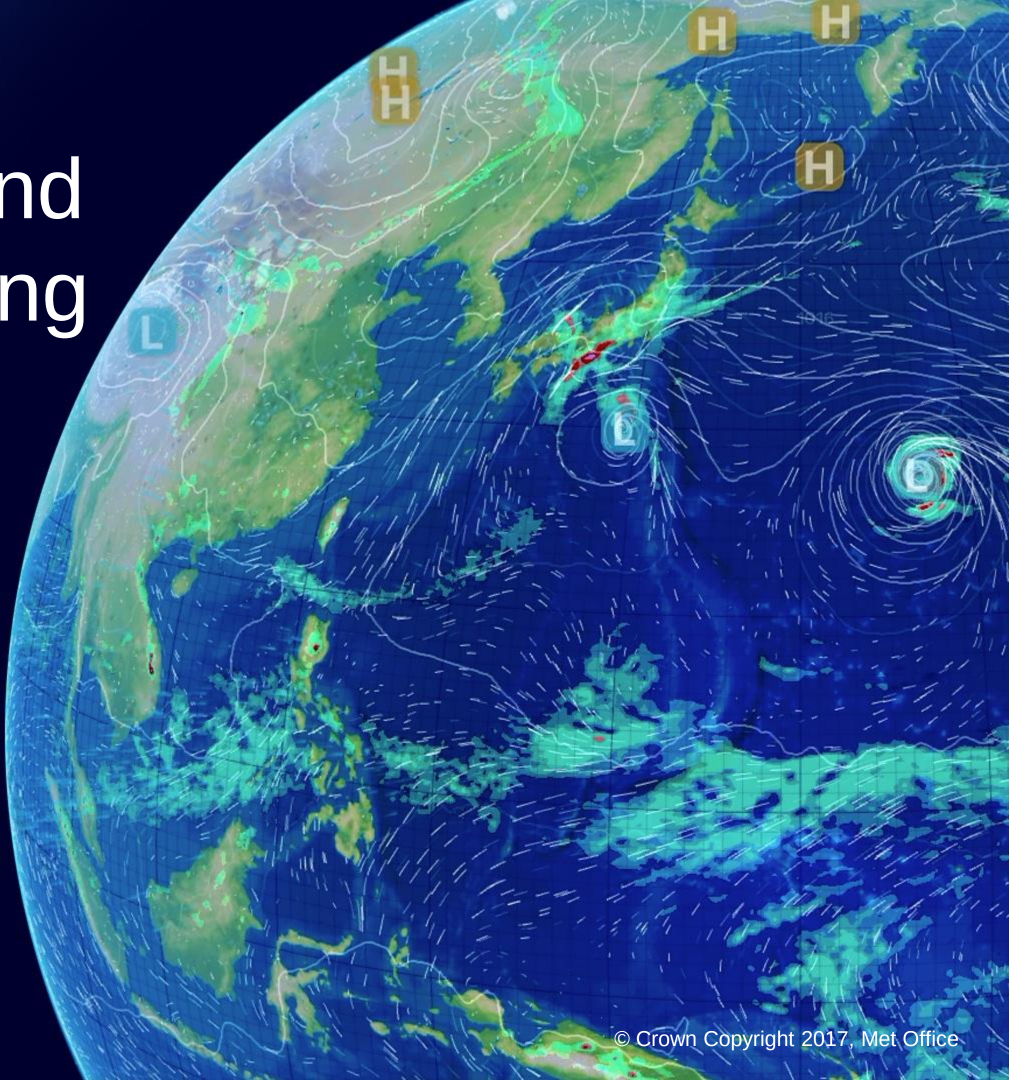

Claudio Sanchez, John Methven,
Sue Gray and Mike Cullen

WCB Workshop.

11/3/2020, ECMWF, Reading, UK

© Crown Copyright 2017, Met Office

Introduction

- Uncertain representation of convective processes at forecast T+0 could **become large errors** at medium-range (e.g ‘forecast bust’ of Rodwell et al 2013)
- The dynamical mechanisms of error amplification are still debated

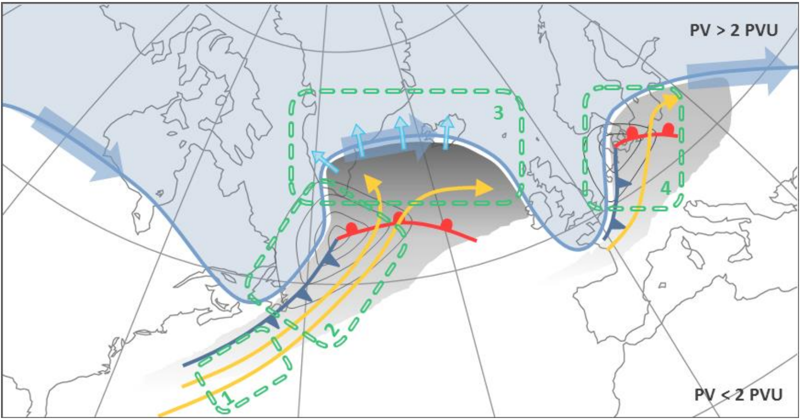

[Top]: Sketch of NAWDEX main goals: Observation of diabatic process in WCB (1,2), ridge formation (3) and downstream effects (4). *From Schäfler et al. (2018, BAMS)*

NAWDEX Hypothesis: Diabatic processes (1,2) have a major influence on the jet stream structure near North Atlantic, affecting the downstream development of Rossby waves (3) and eventually high impact weather (4) over Europe

NAWDEX campaign: Four aircraft observing diabatic processes and ridge development from *15/9* to *22/10* 2016

Met Office

Introduction (2): Goals

Test the NAWDEX hypothesis in three steps

1. Seek evidence for flow-dependent predictability using MetOffice and ECMWF operational forecasts during the NAWDEX period (Sept-Oct 2016).
2. Quantify the diabatic influence on the balanced flow through the **advection of potential vorticity mechanism**, based on a Semi-Geotriptic (SGT) inversion model that provides the ageostrophic flow response to diabatic heating or dynamical sources
3. Test whether or not the situations with lowest predictability are associated with strong diabatic influence.

© Crown Copyright 2017, Met Office

Predictability barriers (1)

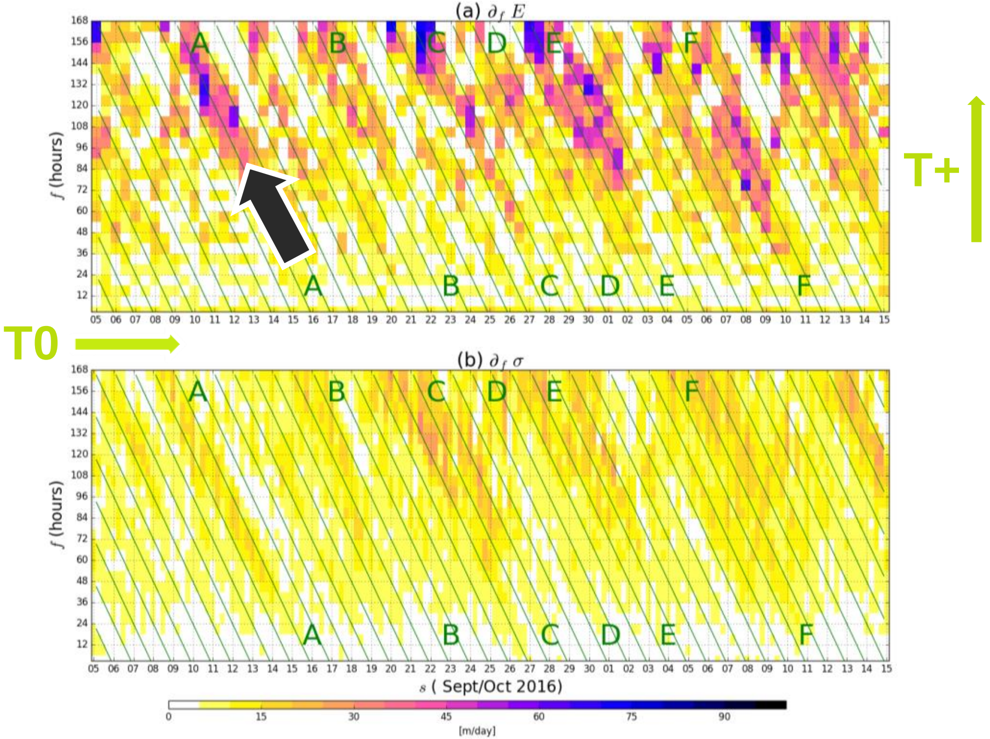

f	Forecast lead time (hours since the start of the forecast)
s	Forecast initialization time
t	Validation time ($s + f$ in forecasts)

There are **times t** where error and spread grows rapidly (UM, IFS), error grows faster than spread (--); E.g. **A** (00Z 16th)

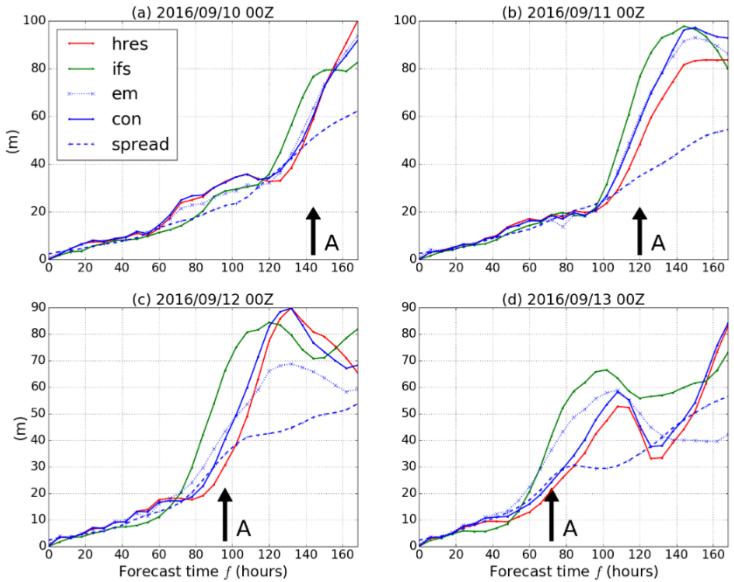

Z500 RMSE rate of change ($\partial E / \partial f$): For all **forecast start dates *s*** and **forecast lead times *f*** *over* NAWDEX Period (15/9 to 15/10). **validation time *t*** on diagonal lines.

Predictability barriers (2)

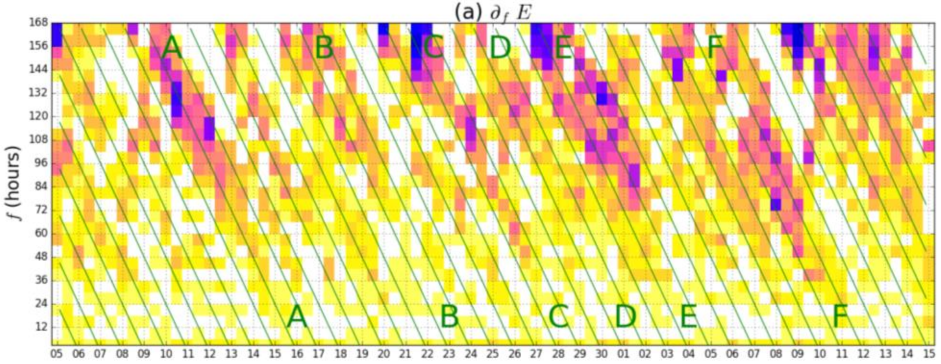

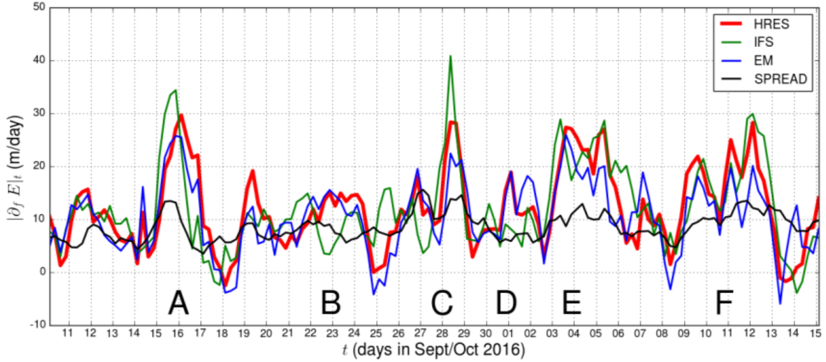

[Top]: *∂E / ∂f* integrated across lead time for same validation time (diagonal lines)

Events with large increase of error growth at a similar validation time are defined as ***predictability barriers (PB)***

- Similar for IFS and UM (HRES)
- Spread growth much smaller than EM error growth during PBs

	HRES	IFS	EM	SPREAD
HRES	·	0.725	0.849	0.488
IFS	·	·	0.608	0.567
EM	·	·	·	0.467

[Top]: Table with Pearson correlation coefficients from left side Figure, all significant at 99% level

PBs coincides with NAWDEX IOPs!

Semi-Geostrophic inversion tool (SGT)

*SGT model able to solve **pressure tendency**, **ageostrophic wind** and **balanced vertical wind (w).** Source term is a linear combination of a **dynamics only** term and **diabatic sources***

- SGT **w** shows induced ascent on the upstream flank of a ridge for TC Ian (1) and downstream cyclone (2)
- Clear signal of diabatic process inducing vertical ascent and divergence over outflow region (d)

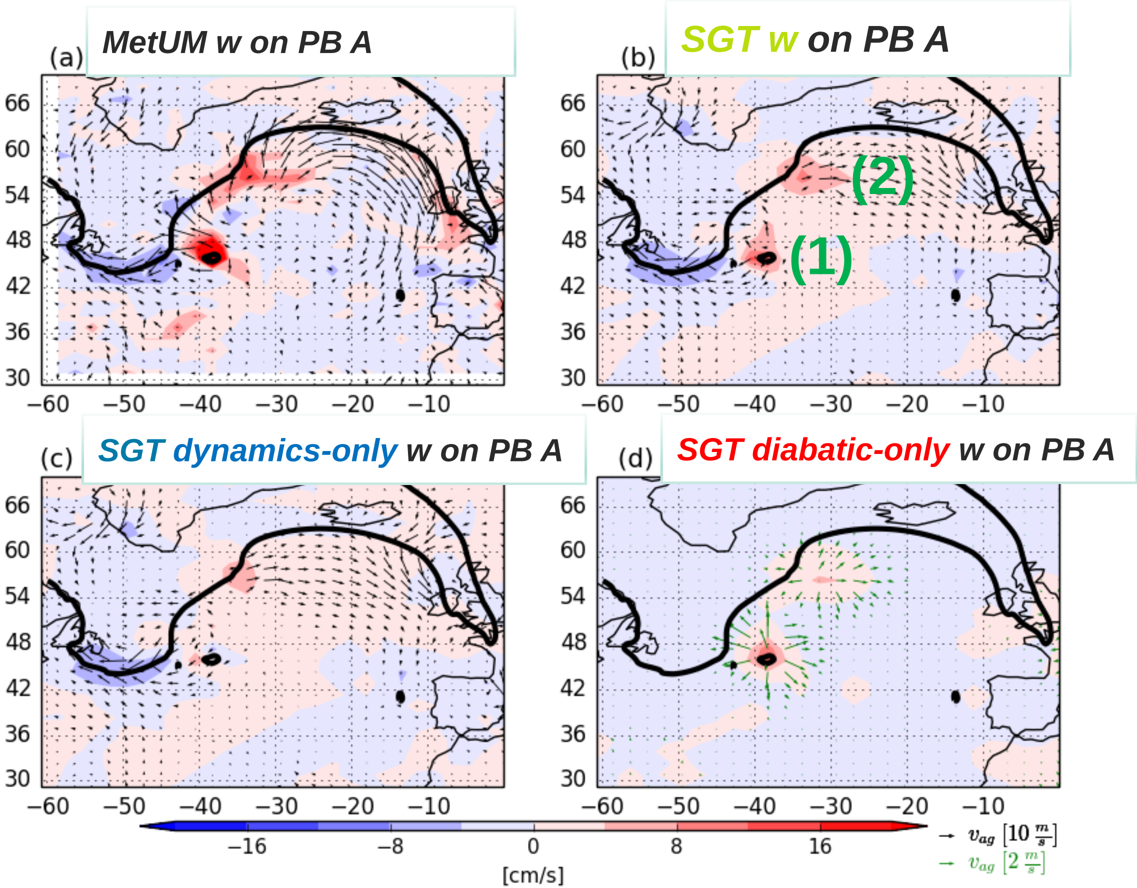

[Top]: SGT *w* (coloured), v_{ag} (vectors) and *PV= 2 PVU* (think black line)

Ageostrophic Advection of PV

Diabatically influenced Ageostrophic Advection of PV (DIAA): PV advected as a result of diabatically induced SG ageostrophic winds.

Dynamic only (or geostrophic) induced ageostrophic advection of PV (SGAA)

- Diabatically influenced (DIAA) shows clearer ridge building action for upstream cyclone (2) (b,d) than SGAA (a,c)
- Degradation of ridge building with forecast lead time (a,b to c,d), domain average value ↓

[Right]: AAPV (coloured) v_{ag} (vectors) and *PV= 2 PVU* (thick black line).

$$AAPV = -v_{ag} \cdot \nabla q$$

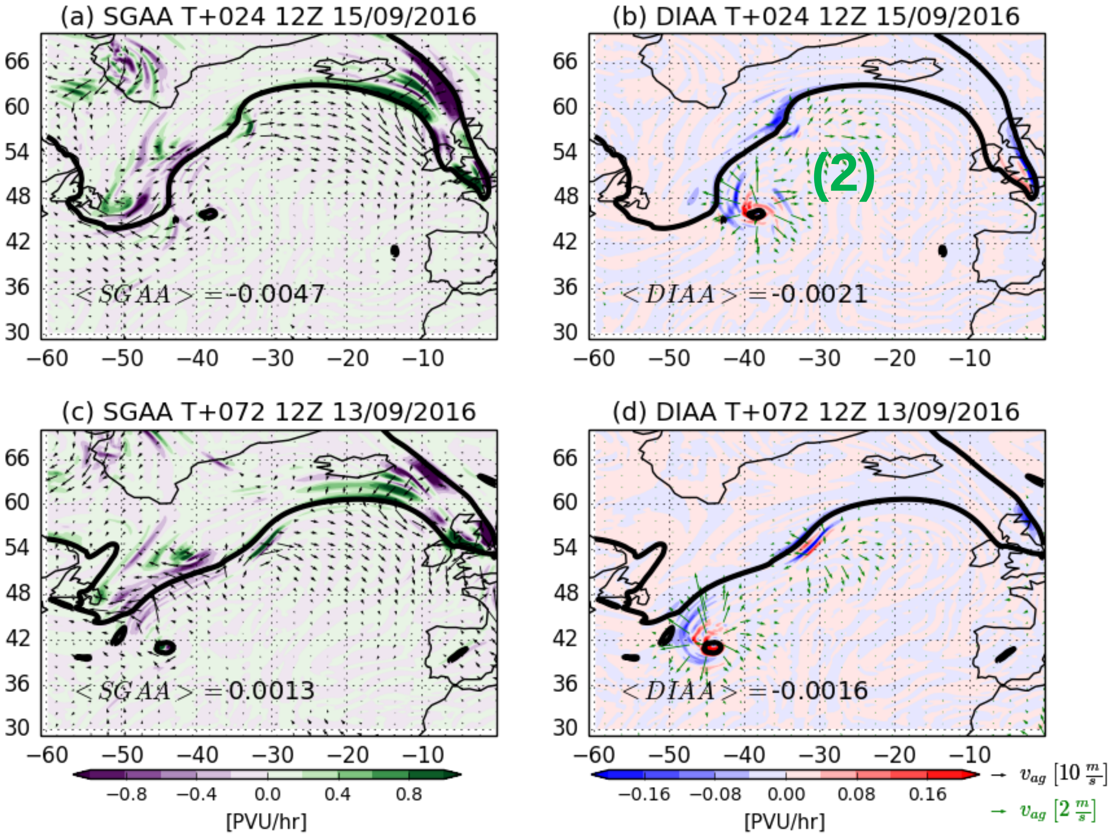

Met Office DIAA in NAWDEX

Diabatic influence DIAA across different PB shows clear ridge building differences between T+24 and T+72

- ***B**, Cyclone Vladiana*
- ***D**, Stalactite Cyclone*
- ***E**, Frontal cyclone*
- ***F**, Thor ridge and cut-off Sanchez*

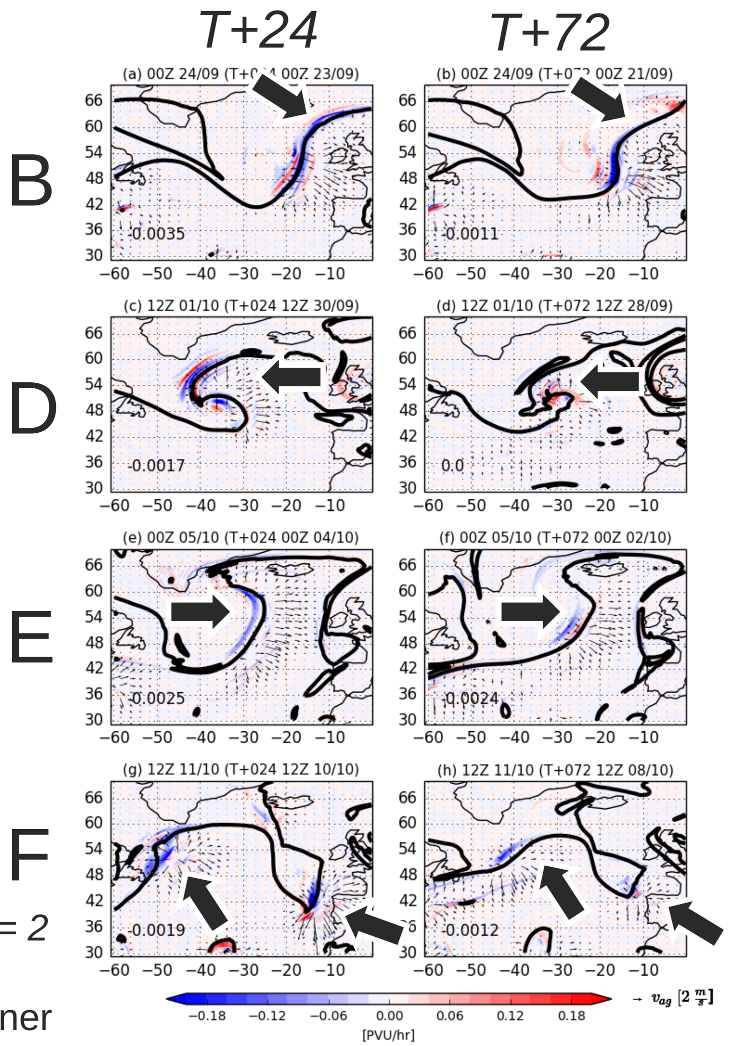

[Right]: *DIAA* (coloured), v_{ag} (vectors) and *PV= 2 PVU* (thick black line).T+24 (left) T+72 (right). Mean value over box shown in bottom-left corner

Diabatic influence and predictability barriers

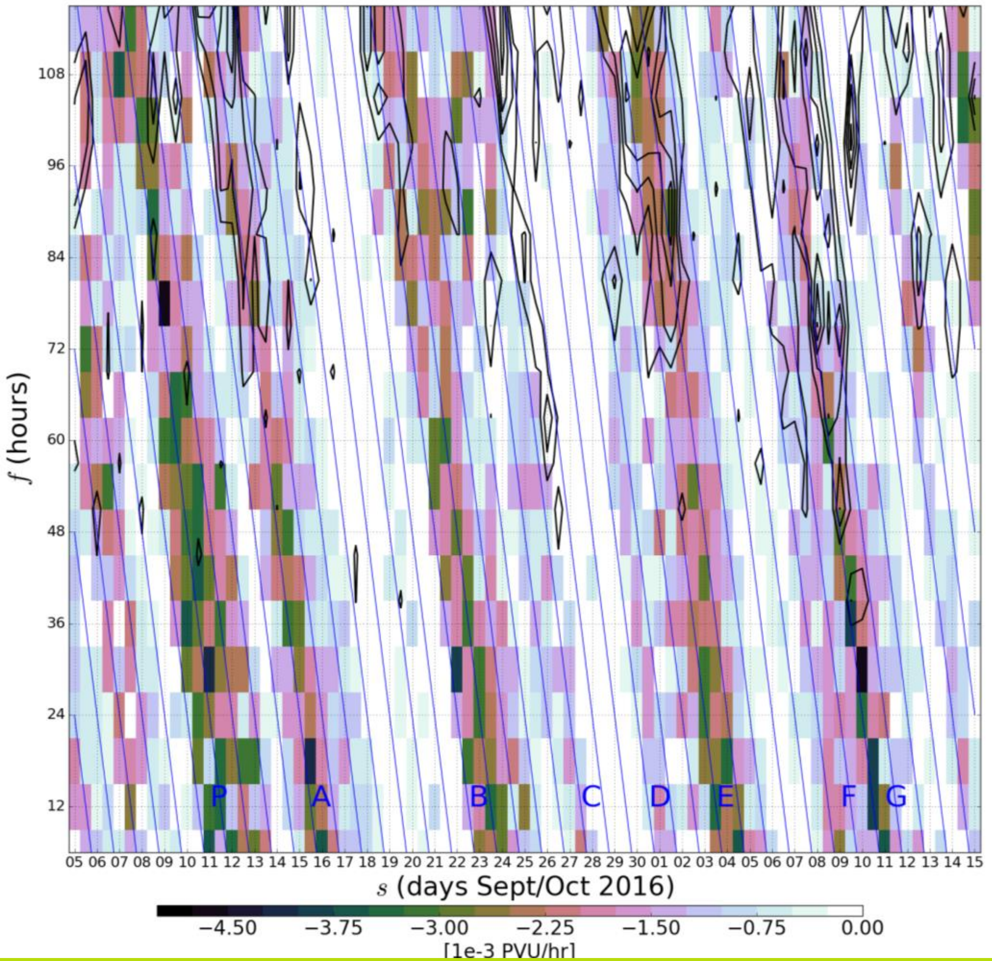

Most of PB cases coincide with high domain averaged Diabatic influence (DIAA); e.g **A, C, E, G**

Some PB cases occur 2 days after high diabatic influence; e.g. **P-A, B-C, D-E, F-G** ("preconditioning environment"?)

[Left] Domain averaged *Diabatic influence (DIAA)* (coloured) and *error growth rate* (contoured)

© Crown Copyright 2017, Met Office

Diabatic influence and predictability barriers (2)

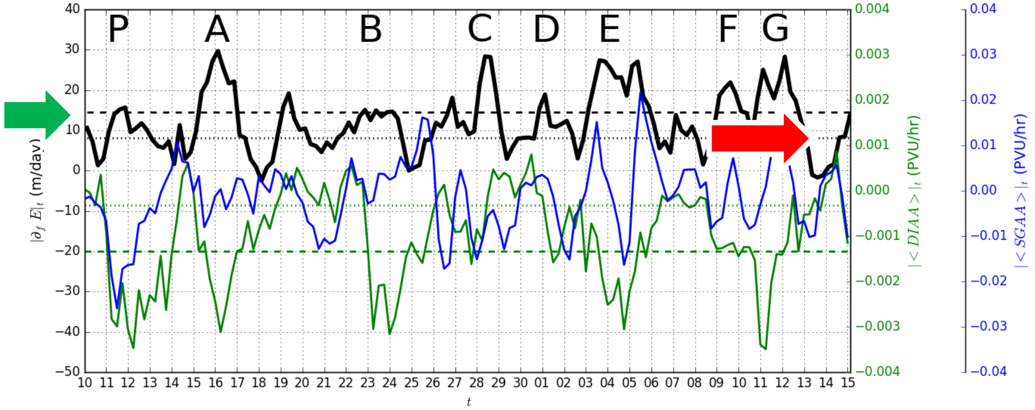

[Left]: Time series of **PB**, **DIAA**, and **SGAA** integrated across t

Time series A	series B	correlation	P-coefficient
$\vert\partial_f E\vert_t$	$\vert<DIAA>\vert_t$	−0.395	< 0.01
$\vert\partial_f E\vert_t$	$\vert<SGAA>\vert_t$	0.028	0.74
$\vert<DIAA>\vert_t$	$\vert<SGAA>\vert_t$	0.121	0.15

[Down]: DIAA vs f for upper (lower) and all PB events (Defined as upper lower tercile of *error growth*)

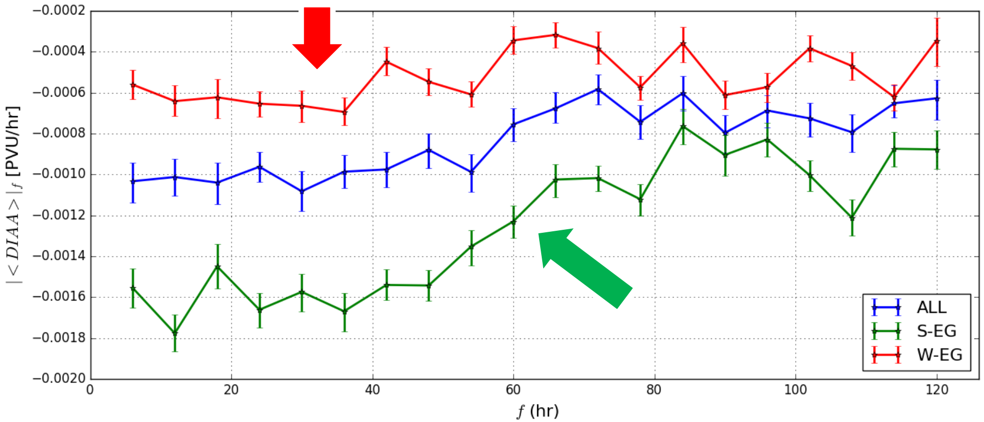

Error growth rate *(PB)* and diabatic influence (*DIAA)* correlation significant, unlike SG influenced (*SGAA)*

DIAA stronger for high strong *error growth* (upper tercile of error growth timeserie), substantial drop when ***f*** > 60 hours

SG and predictability barriers (3)

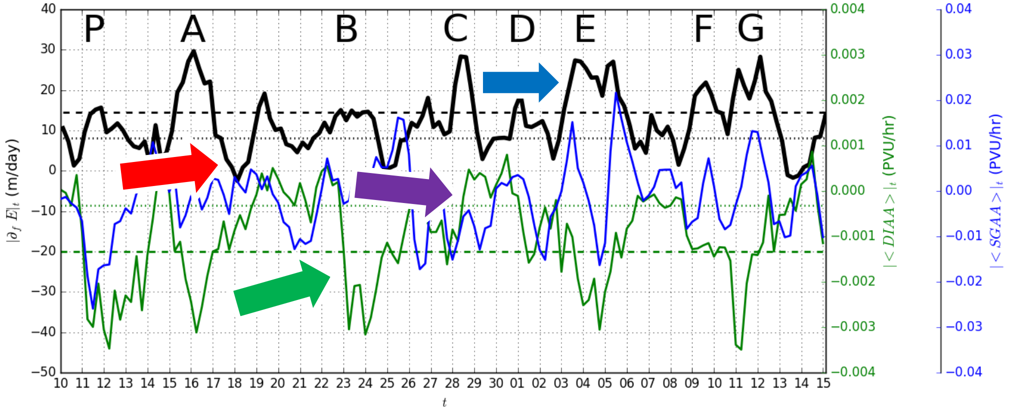

[Top]: Time series of **PB**, **DIAA**, and **SGAA**

Comparing EM error and spread for strong/weak (upper/lower terciles of timeseries) error growth (EG) and diabatic influence (DI):

Spread matches error when diabatic influence is weak.

Error grows 4/3 faster than spread after day 2 when DIAA is strong.

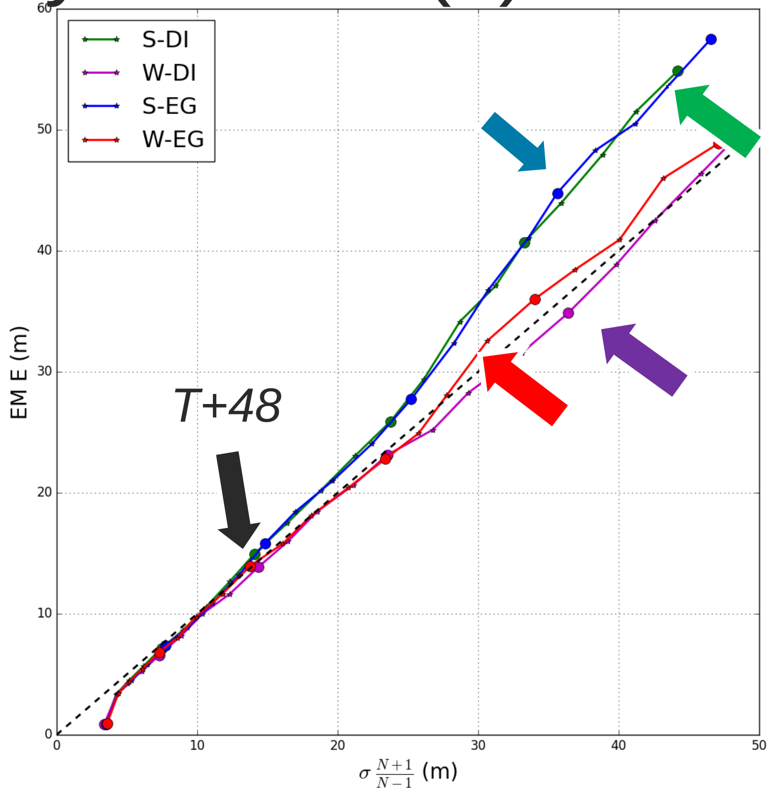

[Top]: MetUM EM RMSE (E) vs spread (σ), for Strong (Weak) Diabatic influence of error growth.

Met Office

Conclusions

- Rapid error and ensemble spread growth was identified on particular dates, irrespective of lead times. *Defined as* ***Predictability Barriers (PB)***
- The Diabatically Induced Ageostrophic Advection of PV (**DIAA**) from SGT model is **strong and negative** in the western flank of developing ridges -> ridge expansion
- Only DIAA is correlated with error growth rate, dynamics-only SGAA is not
- During strong error growth events (PB) :
  - DIAA is ~1.5x larger than average
  - DIAA halves beyond T+60
  - Error growth rate exceeds spread rate beyond T+48

Unresolved questions:

- What are the diabatic processes behind DIAA decrease on PB events?
- Are those processes misrepresented in the model? Are uncertainties in these processes not captured by the ensemble system?

© Crown Copyright 2017, Met Office

Met Office

Thanks for your attention!

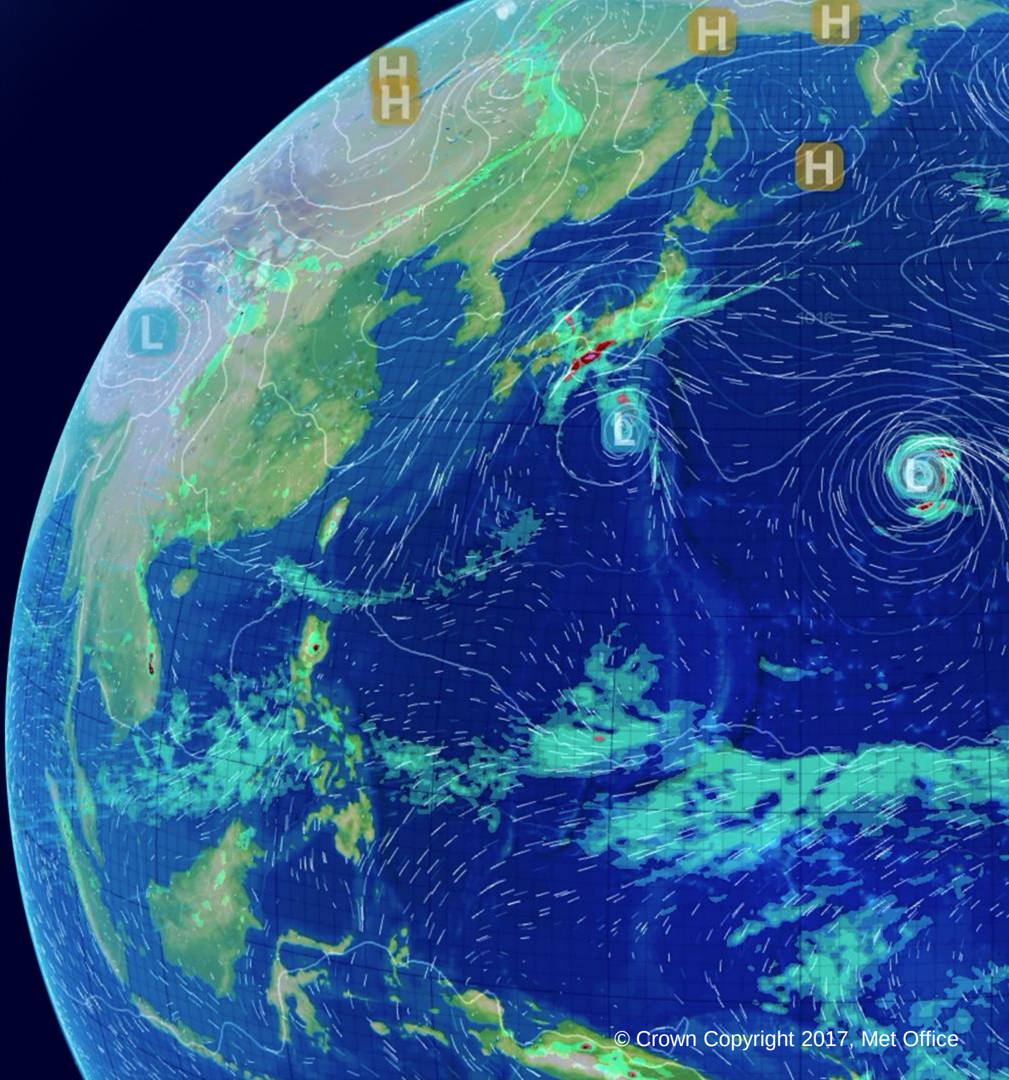

© Crown Copyright 2017, Met Office

Predictability barriers & NAWDEX

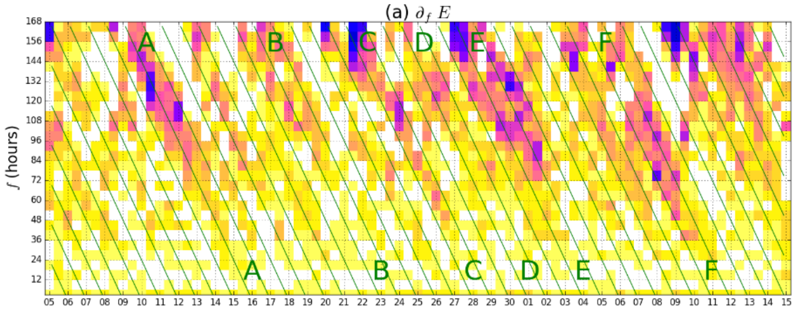

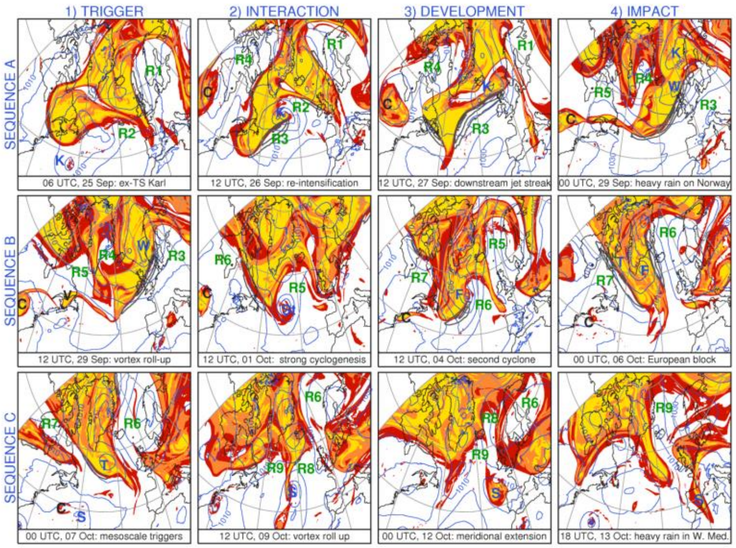

(A): 16th-18th Sept. *Ex-TC Ian*. IOP 1

(B): 22nd-23th Sept. *Vladiana* IOP 4

(C): 28-29th Sept. *Walpurga* + *Ex-TC Karl*. IOP 5

SEQUENCE A

(D): 1st-2nd Oct. *Stalactite cyclone.* IOP 6

(E): 4th-6th Oct. Downstream effects of *Stalactite cyclone* + blocking development. IOP 7

SEQUENCE B

(F): 11-13th Oct. PV cut off *Sanchez* + tropopause ridge *Thor*. IOP 9-10

SEQUENCE C

[Left] NAWDEX golden cases (*aka* Sequences)
Fig 6. Schaffler et al. 2018

Final conclusions and Future work

As hypothesized in NAWDEX campaign: Diabatic processes induce divergent outflow in ridges (2^{nd} stage of error growth of Baumgart et al. 2019), affecting the downstream development of Rossby waves, and thus leading to large forecast error growth (Predictability barriers)

To do …

- What processes are responsible for high values of DIAA over western flank of ridges (e.g. *Joos and Wernli 2012*)?
- Why DIAA declines after day 2?
- Are similar conclusions found in other areas or seasons (e.g. US west-coast)

© Crown Copyright 2017, Met Office

SGT Inversion Model

$$\mathbf{BQ}'\begin{pmatrix} u-u_e \\ v-v_e \\ w \end{pmatrix} + c_{pd}\theta_v \frac{\partial}{\partial t}\begin{pmatrix} \frac{1}{r\cos\phi}\left(\frac{\partial \pi}{\partial \lambda} - \frac{\partial \pi}{\partial r}\frac{\partial r}{\partial \lambda}\right) \\ \frac{1}{r}\left(\frac{\partial \pi}{\partial \phi} - \frac{\partial \pi}{\partial r}\frac{\partial r}{\partial \phi}\right) \\ \frac{\partial \pi}{\partial r} \end{pmatrix} = \mathbf{BH}'$$

$$\mathbf{H}' = \begin{pmatrix} -(\mathbf{u}_e\theta_v)\cdot\nabla\left(\frac{v_e}{\theta_v}\right) + S_v - \frac{v_e S_{\theta_v}}{\theta_v} \\ (\mathbf{u}_e\theta_v)\cdot\nabla\left(\frac{u_e}{\theta_v}\right) - S_u + \frac{u_e S_{\theta_v}}{\theta_v} \\ -\mathbf{u}_e\cdot\nabla\theta_v + S_{\theta_v} \end{pmatrix}$$

SGT model able to solve pressure tendency (dπ/dt), ageostrophic wind ($v - v_e$) and balanced vertical wind (w).

Source Matrix H': linear comb. of geostrophic term plus friction and diabatic sources

SGT improves the Quasi-Geostrophic (QG) model:

- SGT model includes advection by the ageostrophic velocity
- The Ertel PV is conserved by SGT to the order of accuracy of the SGT model in adiabatic and frictionless conditions

SGT ~ SG at the tropopause level, as we do not include source friction in the SGT model and we are above BL

Met Office Semi-Geotriptic (SGT) Inversion Model

UM eqs:

$$\frac{D\mathbf{u}}{Dt} + c_{pd}\theta_v \nabla\pi + 2\Omega \times \mathbf{u} = \mathbf{g} + \frac{\partial}{\partial r}\left(K_m \frac{\partial \mathbf{u}_h}{\partial r}\right) + S_{\mathbf{u}},$$

$$\frac{D\theta_{vd}}{Dt} = S_{\theta_{vd}},$$

\+

Balance eq:

$$c_{pd}\theta_v \nabla_h \pi - (f v_e, -f u_e) = \frac{\partial}{\partial r}\left(K_m \frac{\partial \mathbf{u}_e}{\partial r}\right)$$

$$c_{pd}\theta_v \frac{\partial \pi}{\partial r} = -g.$$

Π: Exner pressure

K_m: BL diffusion coef.

S: Source terms

v_e: Geotriptic wind

$$\mathbf{BQ}'\begin{pmatrix} u - u_e \\ v - v_e \\ w \end{pmatrix} + c_{pd}\theta_v \frac{\partial}{\partial t}\begin{pmatrix} \frac{1}{r\cos\phi}\left(\frac{\partial \pi}{\partial \lambda} - \frac{\partial \pi}{\partial r}\frac{\partial r}{\partial \lambda}\right) \\ \frac{1}{r}\left(\frac{\partial \pi}{\partial \phi} - \frac{\partial \pi}{\partial r}\frac{\partial r}{\partial \phi}\right) \\ \frac{\partial \pi}{\partial r} \end{pmatrix} = \mathbf{BH}'$$

$$\mathbf{H}' = \begin{pmatrix} -(\mathbf{u}_e\theta_v)\cdot\nabla\left(\frac{v_e}{\theta_v}\right) + S_v - \frac{v_e S_{\theta_v}}{\theta_v} \\ (\mathbf{u}_e\theta_v)\cdot\nabla\left(\frac{u_e}{\theta_v}\right) - S_u + \frac{u_e S_{\theta_v}}{\theta_v} \\ -\mathbf{u}_e\cdot\nabla\theta_v + S_{\theta_v} \end{pmatrix}$$

SGT model able to solve pressure tendency (dπ/dt), ageostrophic wind ($v - v_e$) and balanced vertical wind (w).

Source Matrix H’: linear comb. of geostrophic term plus friction and diabatic sources

Semi-Geostrophic Inversion Model

$$\mathbf{B}\mathbf{Q}'\begin{pmatrix} u-u_e \\ v-v_e \\ w \end{pmatrix} + c_{pd}\theta_v\frac{\partial}{\partial t}\begin{pmatrix} \frac{1}{r\cos\phi}\left(\frac{\partial\pi}{\partial\lambda}-\frac{\partial\pi}{\partial r}\frac{\partial r}{\partial\lambda}\right) \\ \frac{1}{r}\left(\frac{\partial\pi}{\partial\phi}-\frac{\partial\pi}{\partial r}\frac{\partial r}{\partial\phi}\right) \\ \frac{\partial\pi}{\partial r} \end{pmatrix} = \mathbf{B}\mathbf{H}'$$

Where

$$\mathbf{B} = \begin{pmatrix} f & -\frac{\partial}{\partial r}\left(K_m\frac{\partial}{\partial r}\right) & 0 \\ \frac{\partial}{\partial r}\left(K_m\frac{\partial}{\partial r}\right) & f & 0 \\ 0 & 0 & g/\theta_v \end{pmatrix}$$

$$\mathbf{Q}' = \begin{pmatrix} f+\frac{\theta_v}{r\cos\phi}\frac{\partial}{\partial\lambda}\left(\frac{v_e}{\theta_v}\right)+\frac{u_e\tan\phi}{r} & \frac{\theta_v}{r}\frac{\partial}{\partial\phi}\left(\frac{v_e}{\theta_v}\right)+\frac{\partial}{\partial r}\left(K_m\frac{\partial}{\partial r}\right) & \theta_v\frac{\partial}{\partial r}\left(\frac{v_e}{\theta_v}\right) \\ -\frac{\theta_v}{r\cos\phi}\frac{\partial}{\partial\lambda}\left(\frac{u_e}{\theta_v}\right)+\frac{v_e\tan\phi}{r}-\frac{\partial}{\partial r}\left(K_m\frac{\partial}{\partial r}\right) & f-\frac{\theta_v}{r}\frac{\partial}{\partial\phi}\left(\frac{u_e}{\theta_v}\right) & -\theta_v\frac{\partial}{\partial r}\left(\frac{u_e}{\theta_v}\right) \\ \frac{1}{r\cos\phi}\frac{\partial\theta_v}{\partial\lambda} & \frac{1}{r}\frac{\partial\theta_v}{\partial\phi} & \frac{\partial\theta_v}{\partial r} \end{pmatrix}$$

Elliptic equation for

$\partial\pi/\partial t$ →

$$\frac{\kappa_d-1}{\kappa_d}\frac{\rho_d}{\pi}r^2\frac{\partial r}{\partial\eta}\frac{\partial\pi}{\partial t}+r^2\frac{\partial r}{\partial\eta}\frac{\rho_d c_{pd}\theta_v^2}{g\theta_{vd}}\frac{\partial}{\partial t}\left(\frac{1}{(1+\mu)}\frac{\partial\pi}{\partial r}\right)+\nabla\cdot\left(r^2\rho_d c_{pd}\theta_v\frac{\partial r}{\partial\eta}\mathbf{R}\mathbf{P}^{-1}\frac{\partial}{\partial t}(\nabla_r\pi)\right)=$$
$$\nabla\cdot\left(r^2\rho_d\frac{\partial r}{\partial\eta}\mathbf{R}\mathbf{P}^{-1}\mathbf{G}\right)+\frac{1}{\cos\phi}\left(\frac{\partial}{\partial\lambda}\left(r\rho_d u_e\frac{\partial r}{\partial\eta}\right)+\frac{\partial}{\partial\phi}\left(r\rho_d v_e\cos\phi\frac{\partial r}{\partial\eta}\right)\right).$$

[Improvements to S-G omega equation …]

Its form in momentum coordinates (Hoskins & Draghici, 1977) is:

$$\nabla_X^2\left(\frac{g\rho_r}{\theta_0 f_0}q_g w^*\right)+f_0^2\frac{\partial^2 w*}{\partial Z^2}=2\nabla_X.\mathbf{Q}+\nabla_X^2 H \qquad H=\alpha w^*, \qquad \hat{Z}=\frac{N_0}{f_0}Z$$

Geostrophic forcing

Diabatic forcing (H=heating)

© Crown Copyright 2017, Met Office

Predictability barriers

ACC as function of start and valid time

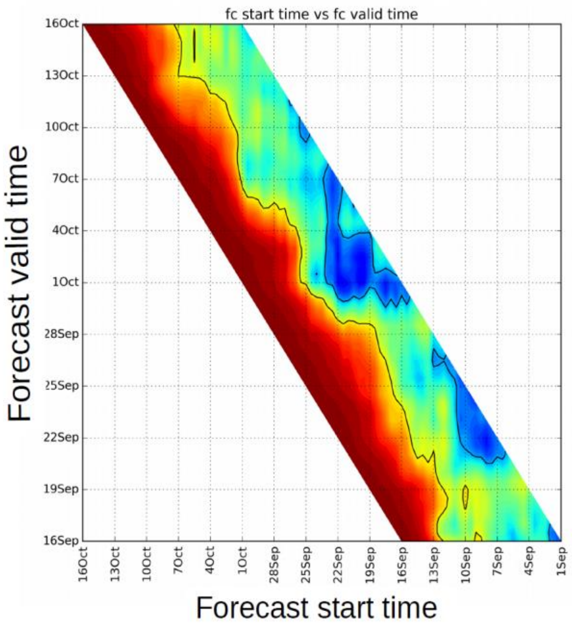

Rate of change of ACC

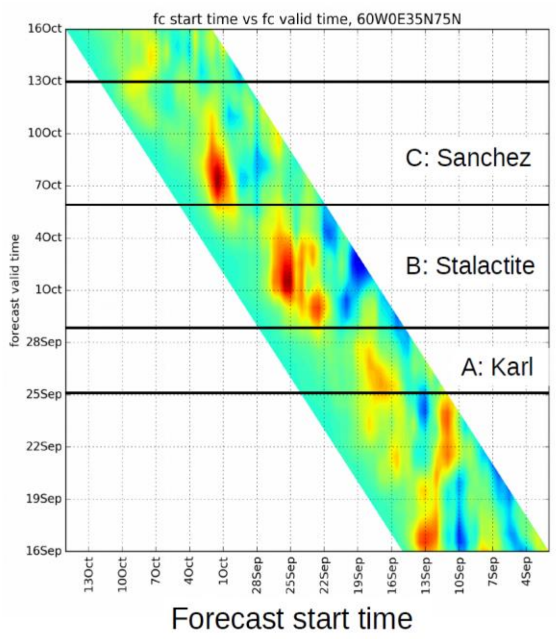

Rate of change of *ACC* for *IFS* *Z500* ***increases at particular validation times***, defined as ***"predictability barriers"***

Craig et al. (2018): Predictability barriers, *NAWDEX 2018 workshop, Munich*

© Crown Copyright 2017, Met Office

SG and predictability barriers (+)

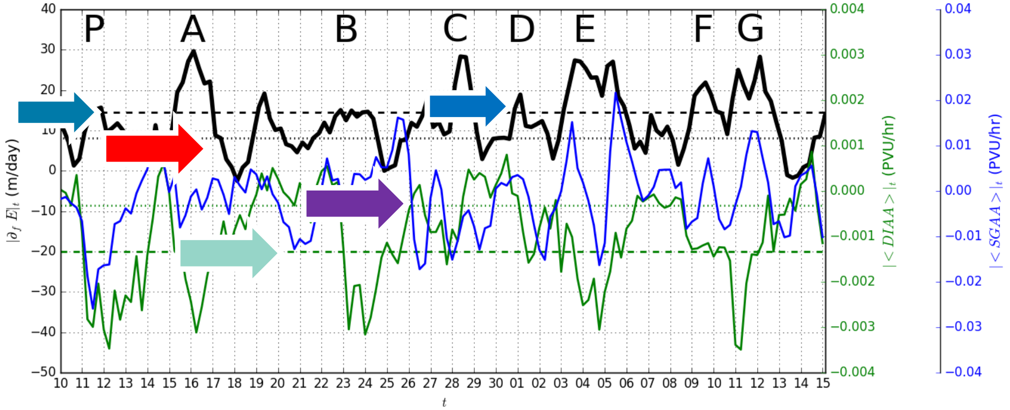

[Left]: Time series of **PB**, **DIAA**, and **SGAA**

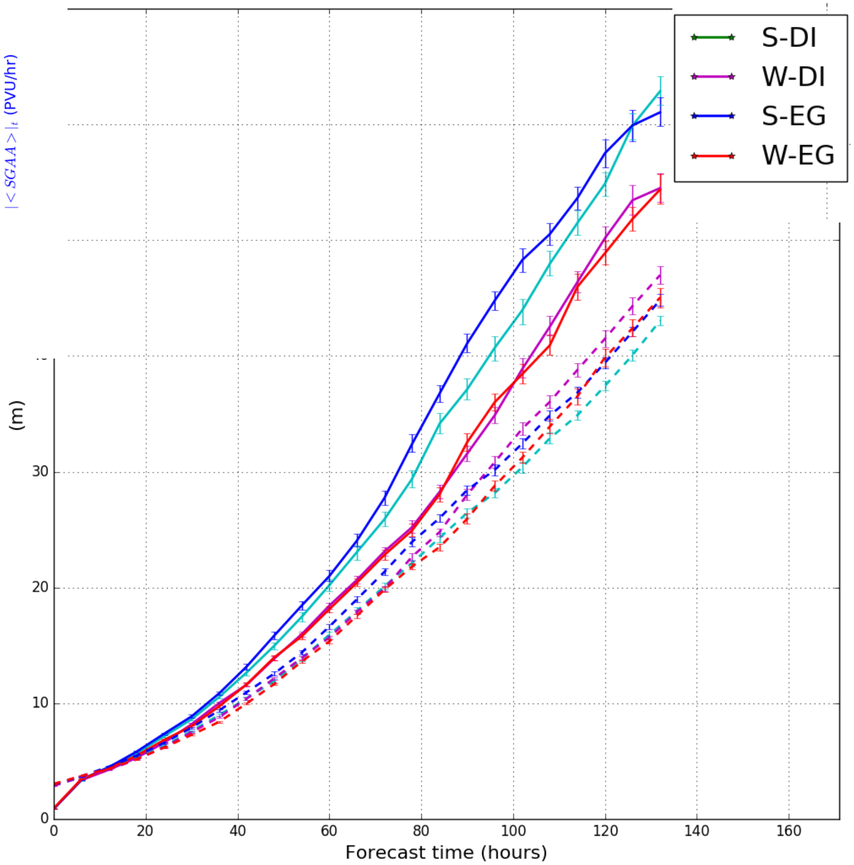

[Left]: N768 EM RMSE (*E*,-) ad spread (*σ*,--), for High (Non) Non-Diabatic Influence or PB. Def as upper (lower) threshold in PB and DI-AAPV timeseries

DIAA sketch

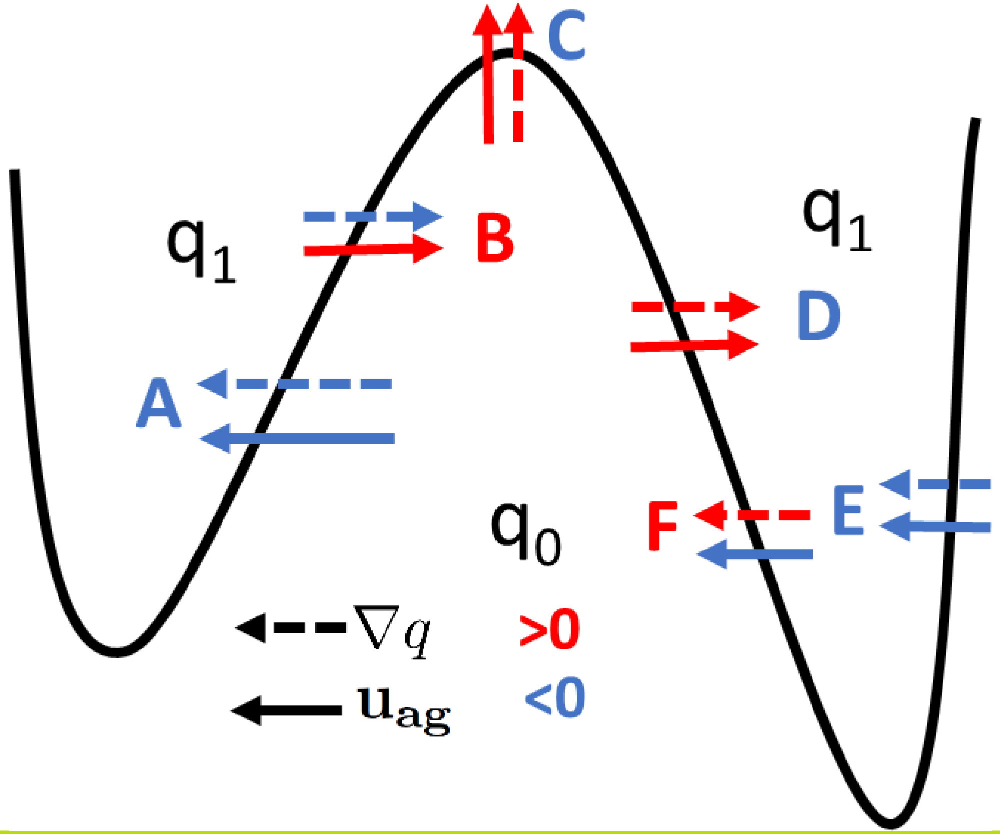

$$AAPV = -v_{ag} \cdot \nabla q$$

A,C,D,E: SG wind parallel to PV gradient (troposphere advecting towards stratosphere): DIAA negative

B,F: SG wind antiparallel to PV gradient, DIAA positive

© Crown Copyright 2017, Met Office

Thoughts on Predictability Barriers

For a reliable forecast spread should match EM error for all lead times averaged over many forecast dates. Reasons why forecast error growth may be larger than ensemble spread during PB events:

1. Stochastic physics and ensemble design of initial condition uncertainty do not capture well major sources of model error that makes the rapid error growth during PB events
2. Very low predictability of PB events, flow may follow a very unlikely path

© Crown Copyright 2017, Met Office

Met Office

Methodology

Operational Models employed to spot Error growth:

- Met Office Unified Model (MetUM, H-Res) operational deterministic model (N768 ~18km, L70, GA6.1)
- Integrated Forecast System (IFS) operational deterministic model (O1280 ~9 km, L137, Cy41r2)
- Global MetUM operational Ensemble Prediction System (MOGREPS-G, N400,~35km, L70, GA6.1, 24 members)

H-Res re-run with the necessary diagnostics to run the Semi-Geotripctic inversion model 6 hourly up to T+120